International Journal of Nanoelectronics and Materials
IJNeaM
ISSN 1985-5761 | E-ISSN 2232-1535

Dependency of depletion capacitance on switching threshold of an inverter

Sumi Baby [a] * and Anju Pradeep [a]

[a]*School of Engineering, CUSAT, KOCHI, 682022, India*
∗Corresponding author. Tel.: +9894114220; e-mail: sumibaby@cusat.ac.in

Received 30 March 2026, Revised 28 April 2026, Accepted 20 May 2026

ABSTRACT

Depletion capacitance of a Metal Oxide Semiconductor Field Effect Transistor (MOSFET) is a critical parameter that determines the switching threshold of an inverter. The study of this dependency is lacking in the literature. This challenge is addressed by demonstrating a prerequisite for effectively modulating the Hole Concentration (HC) in the channel towards the bulk region of the Zener Tunnelling Tunnel Diode Partially Depleted Silicon On Insulator (ZT-TDPDSOI). The modulation of HC facilitates a variable capacitance effect, leading to a reduction in the subthreshold swing (SS). Fermi level (FL) and electric field analyses are conducted to investigate the variation in HC and the resultant change in capacitance. Furthermore, the effect of the bulk potential, originating from the variation in HC at the drain-channel junction, is revealed. FL and Valence Band Energy (VBE) are used to explain the concentration variation within the channel near the drain-channel region. Doping of P^+ region below source/drain modulates the HC in the channel. The HC extracted from energy band diagram is validated through box profile approximation (BPA). ZT-TDPDSOI is implemented in the inverter circuit and verified the increase in the switching threshold and transition slope there by increasing the efficiency of inverter. Transfer characteristics of inverter is analysed here. There is 12% increase in switching threshold, 4% increase in transition slope and 8% reduction in risetime in ZT-TDPDSOI. All simulations are performed using atlas and mixed signal Technology Computer Aided Design (TCAD).

Keywords: *Inverter, Box profile approximation (BPA), ZT-TDPDSOI, Valence band energy (VBE), Fermi level (FL), Hole concentration (HC)*

1. INTRODUCTION

Designing digital switches with Metal Oxide Semiconductor Field Effect Transistors (MOSFETs) considers speed and power as important performance metrics. These are related to the device parameters such as sub-threshold swing (SS) and OFF current (I_{OFF}) respectively [1–3]. SS should be small for faster switching of MOSFET. The depletion capacitance in the sub-threshold region plays an important role to determine SS in FET used for digital switch as shown in Equation (1) [4–7]:

$$SS = \ln(10) \cdot qkT\left(1 + \frac{C_d}{C_{ox}}\right) \quad (1)$$

where c_d is the depletion capacitance and c_{ox} is oxide capacitance [8–11]. The introduction of P^+ region below source/drain in Zener Tunnelling Tunnel Diode Partially Depleted Silicon On Insulator (ZT-TDPDSOI) changes the uniform doping in the channel and it modulates the Hole Concentration (HC) near the drain-channel region leading to variation in c_d [12–18]. This change in HC has significant effect on SS. Hence an accurate model for HC is essential for the analysis of ZT-TDPDSOI at drain-channel region.

Previous works [19, 20] detailed the reduction in I_{OFF} and SS achieved by incorporating a P^+ region beneath the source/drain. The underlying reasons for these variations attributed to the P^+ region are elaborated in [21]. However, the requirement for getting the HC modulation effect in the bulk is not studied in the prior work, also the P^+ effect is not modelled for properly quantifying the analysis. Dependence of P^+ on HC at drain-channel region is also not verified previously. Therefore, in this paper we demonstrate the prerequisites for achieving HC modulation via bulk potential and electric field behaviour as a function of the doping concentration of P^+. The HC derived from the energy band diagram is validated using the box profile approximation (BPA). In the literature, BPA is used to find the average doping in the channel with a non-uniform doping profile at the surface to model the threshold voltage [3]. The average doping concentration changes when the P^+ is introduced in ZT-TDPDSOI. To understand the variation of HC, it is necessary to analyse the factors that affect the range in concentration.

Depletion capacitance of a MOSFET is a critical parameter that determines the switching threshold of an inverter [22–26]. The study of this dependency is lacking in the literature. To accurately model the effect of P^+ region introduced below source/drain region, it is necessary to understand the underlying, mechanism of variation of HC near the drain-channel region. These challenges are addressed in this paper, BPA is used to find the average doping in the bulk region. The relation of P^+ with the concentration at drain-channel region has been investigated using VBE and FL.

This article is organized as follows: Section 2 presents the valence band and Fermi level of PDSOI and ZT-TDPDSOI. Section 3 observes the HC Comparison of PDSOI, ZT-TDPDSOI at the drain-channel region. Section 4 details the estimation of average doping in ZT-TDPDSOI by modelling the effect of the P^+ and N^+ regions using BPA. Section 5 discusses the electric field distribution along the PP^+ region for various doping concentrations of P^+. Section 6 explores implementation of inverter circuit using ZT-TDPDSOI. Finally, the conclusion is provided in Section 7.

2. METHODOLOGY

Firstly, the Electric field distribution along PP^+ region at the drain-channel region for varying doping concentration of P^+ at different positions is estimated. Secondly the conduction band at P^+P drain-channel region for varying P^+ doping concentration is conducted. After that HC is extracted the at the drain-channel region due to P^+ region for various doping condition.

The variation in HC at drain channel region is validated using the effect of bulk potential and the relationship of P^+ doping with HC is demonstrated using the following procedure.

Comparison of HC corresponding to PDSOI and ZT-TDPDSOI is carried out first. Bulk potential is derived from VBE and FL diagram.

HC validation is done using model equations and simulation results. To find the average doping in the bulk region due to P^+ region below source/drain BPA is applied. Finally the effect of P^+ doping with HC is estimated.

The schematic representation of Zener tunnelling tunnel diode partially depleted silicon on insulator (ZT-TDPDSOI) is shown in Figure 1 [19]. All the simulations are done using TCAD [27]. The drain/source are split into N^+ and P^+ regions. The thickness of P^+ region is 0.05 µm and the doping concentration is 2×10^{20} cm^{-3}. The source/drain junction depth is 0.1 µm and the doping concentration is 10^{20} cm^{-3} each. Length of source/drain is 1 µm. The channel length is 1 µm and doping concentration is 10^{17} cm^{-3}. The device dimensions are given in Table 1.

2.1. Valence Band and Fermi Level of PDSOI and ZT-TDPDSOI

Figure 2 illustrates the energy difference between FL and VBE. The decrease in this energy difference from 0.335 eV (PDSOI) to 0.135 eV (ZT-TDPDSOI) indicates an increase in HC within the drain-channel region. As depicted in Figure 3, the bulk potential can be inferred from the separation between the FL and VBE. The estimation of the bulk potential from the VBE and FL for both PDSOI and ZT-TDPDSOI is detailed below.

Workfunction (ϕ_f) of the device is given by [3]:

$$\phi_f = \psi + E_g - (E_f - E_v) \quad (2)$$

where ψ is the silicon affinity, E_g is the band gap of silicon, $E_F - E_V$ is the distance between FL and VBE. Bulk potential is given by:

$$\phi_b = \phi_f - \psi \quad (3)$$

where ϕ_b bulk potential which is equal to $E_F - E_i$.

Table 1. Device dimension

Region	Dimension and Doping		
	Lateral (µm)	Vertical (µm)	Doping (cm^{-3})
Source	1	N^+ = 0.100	10^{20}
		P^+ = 0.050	2×10^{20}
Drain	1	N^+ = 0.100	10^{20}
		P^+ = 0.050	2×10^{20}
Silicon-on-Insulator Thickness	1	0.200	10^{17}
Gate oxide	1	0.017	-
Buried oxide	3	0.400	-

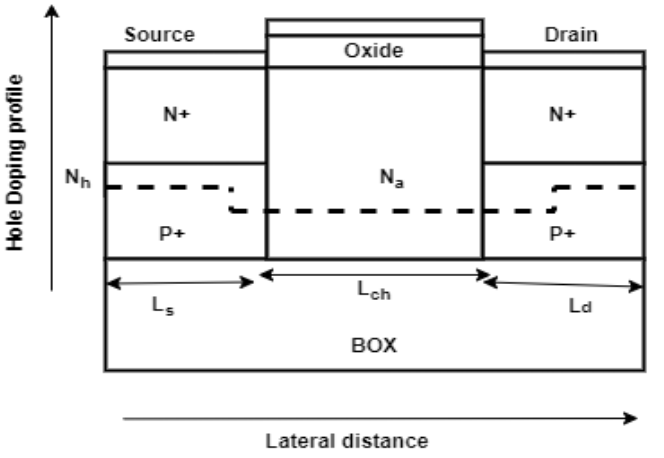

Figure 1. Hole doping profile of ZT-TDPDSOI to implement BPA approximation

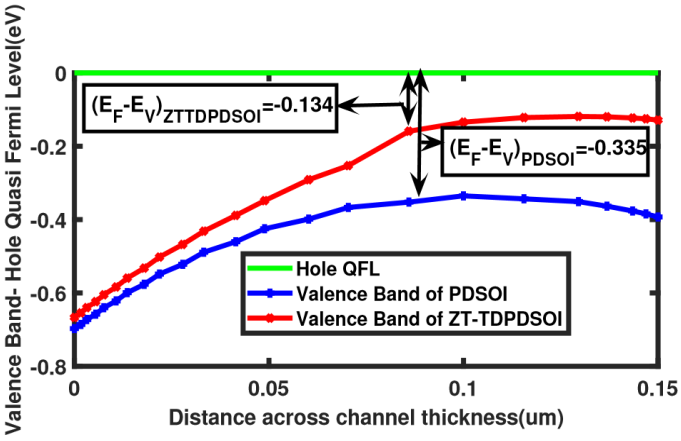

Figure 2. Distance between VBE and hole Quasi fermi level (QFL) for ZT-TDPDSOI and PDSOI at V_{DS} = 0 V V_{GS} = 0 V, to show the difference in potential, cutline is drawn across the channel thickness near the drain channel region

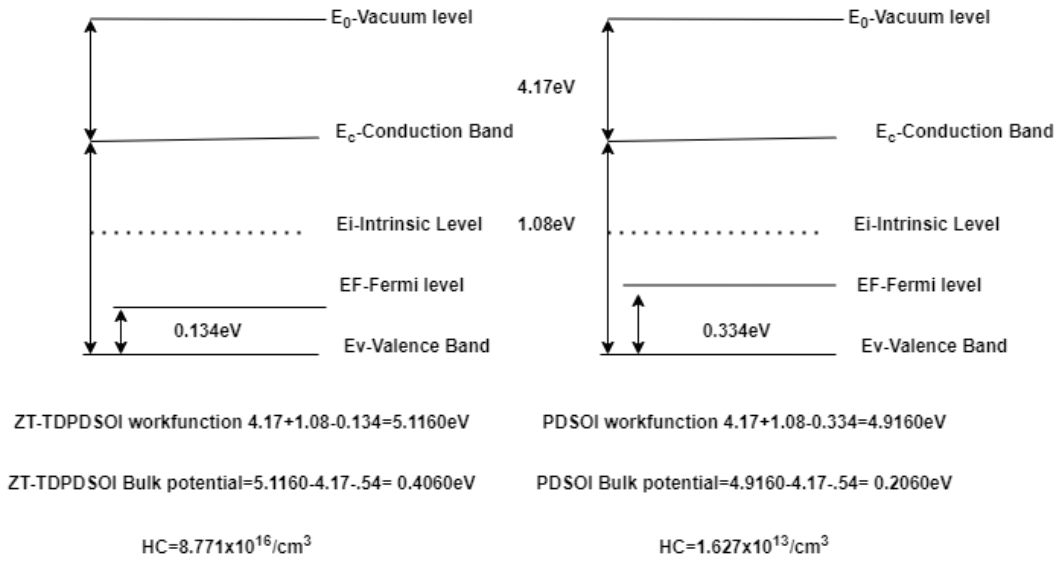

Figure 3. Comparison of bulk potential calculation using E_F-E_V in energy diagram of ZT-TDPDSOI and PDSOI to compare the bulk potential which helps to derive HC

The workfunction (ϕ_f), bulk potential and HC are extracted for both ZT-TDPDSOI and PDSOI as shown in Figure 3. Bulk potential ($E_f - E_i$) for ZT-TDPDSOI is 0.4060 eV and that for PDSOI is 0.2060 V. This is obtained from energy band diagram in Figure 3. There is an error of 2% observed in this case of PDSOI and ZT-TDPDSOI. The increase in HC which results in the reduction of distance between FL and VBE is shown in the next section. Bulk potential obtained from HC and that obtained from energy band diagram (FL, VBE) are compared.

3. HC COMPARISON OF PDSOI, ZT-TDPDSOI AT THE DRAIN-CHANNEL REGION

As previously mentioned, the difference is VB and FL is observed due to the HC variation near drain-channel. This is depicted in Figure 4. The HC at drain-channel region is increased from 2.39 × 10^{13} cm^{-3} to 5.75 × 10^{16} cm^{-3} when P^+ is introduced below source/drain (ZT-TDPDSOI) at equilibrium condition (V_{DS} = 0 V, V_{GS} = 0 V). The HC is increased by a factor of 2405.

From Boltzmann equation bulk potential is given as [3]:

$$E_F - E_i = KT * \ln\frac{p}{n_i} \quad (4)$$

where n_i is intrinsic carrier concentration, P is the HC, E_F is FL, E_i is the intrinsic energy level, KT is the thermal energy. The HC(P) values obtained from Figure 4 which are 3.39 × 10^{13} cm^{-3} for PDSOI and 5.75 × 10^{16} cm^{-3} for ZT-TDPDSOI), are substituted in Equation (4). The bulk potential thus obtained is 0.2016 V for PDSOI and 0.3950 V for ZT-TDPDSOI. The increase of HC at drain channel region causes reduction of gap between VBE and hole QFL ($E_F - E_V$) of ZT-TDPDSOI compared to PDSOI. The bulk potential obtained from VB, FL and HC are comparable. The comparison of bulk potential obtained from VB and FL and from HC near drain-channel region confirms the fact that the reason for VB, FL variation is due to HC variation in near the drain-channel region. The details are shown in Table 2.

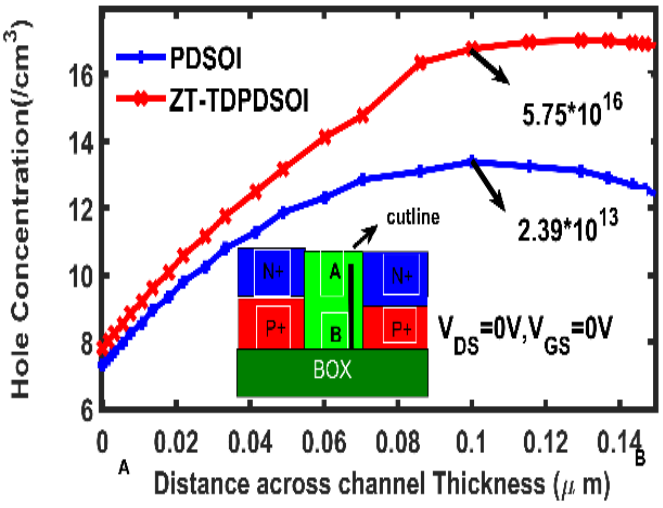

Figure 4. Comparison of HC as a function of channel thickness of PDSOI and ZT-TDPDSOI. The concentration increases from 2.39 × 10^{13} cm^{-3} to 5.75 × 10^{16} cm^{-3}

Table 2. Estimation of bulk potential from HC and VBE, FL at drain-channel region

	$E_F - E_v$ (eV)	ϕ_b using HC (V)	ϕ_b using VBE and hole FL (V)	%error = $\frac{\phi b_s - \phi b_c}{\phi b_s}$ (%)
ZT–TDPDSOI	0.134	0.3950	0.4060	2
PDSOI	0.334	0.2016	0.2060	2

ϕb_s: Simulated ϕ_b, ϕb_c: Calculated ϕ_b

4. ESTIMATION OF AVERAGE DOPING BY MODELLING THE EFFECT OF P+ AND N+ IN ZT-TDPDSOI USING BPA

The variation of HC in the drain-channel region causes the change in average doping in the bulk region resulting in the reduction of distance between VBE and FL. The presence of P+ doping below source/drain increases the average doping in the bulk region. This average doping is estimated using source/drain to find the average doping BPA as follows.

Figure 5 shows the BPA for non-uniform doping with P+ or N+ below source/drain. It is divided into three regions:

(i) Area of Region 1 is given as:

$$\text{Region1} = N_h * L_S \tag{5}$$

where N_h is the heavy doping of P+ below source/drain region, L_S is the length of source region.

(ii) Area of Region 2 is given as:

$$\text{Region2} = N_h * L_D$$

where L_D is the length of drain region.

(iii) Area of region 3 is given as:

$$\text{Region3} = N_a * L_{ch}$$

where L_{ch} is the length of channel and N_a the doping concentration in the channel region. Total area is given as:

$$\text{Total area} = \text{Region1} + \text{Region2} + \text{Region3}$$

$$\text{Total area} = N_h * L_S + N_h * L_D + N_a * L_{ch}$$

Here, length of source and drain are equal, therefore we can write:

$$L_S = L_D = L_T \tag{6}$$

Distribute the extra dopant to get an average increment in doping:

$$\text{Total area} = 2 * N_h * L_T + N_a * L_{ch} \tag{7}$$

It is distributed evenly over total length as:

$$f' = \frac{2 * N_h * L_T + N_a + L_{ch}}{2 * L_T + L_{ch}}$$

The increase as compared to the previous doping, the factor that represent the increment is given by:

$$f' = \frac{2 * N_h * L_T + N_a * L_{ch}}{(2 * L_T + L_{ch}) * N_a} \tag{8}$$

Calculated and expected value of *f* factor at drain-channel region is given in Table 3. The average doping for different doping of P+ is shown in Table 4. When the region below drain and source is given N+ the term N_h become zero and the factor reduce to 0.3.

Table 3. Calculated and expected value of f factor at drain-channel region

$(E_F - E_v)$ PDSOI (eV)	$(E_F - E_v)$ ZT–TDPDSOI (eV)	ΔE (s)	ΔE (Equation (11)) (m)	Error (%)
0.334	0.134	0.2	0.187	6

$\Delta E(s)$: Simulation, $\Delta E\ (m)$: modelling

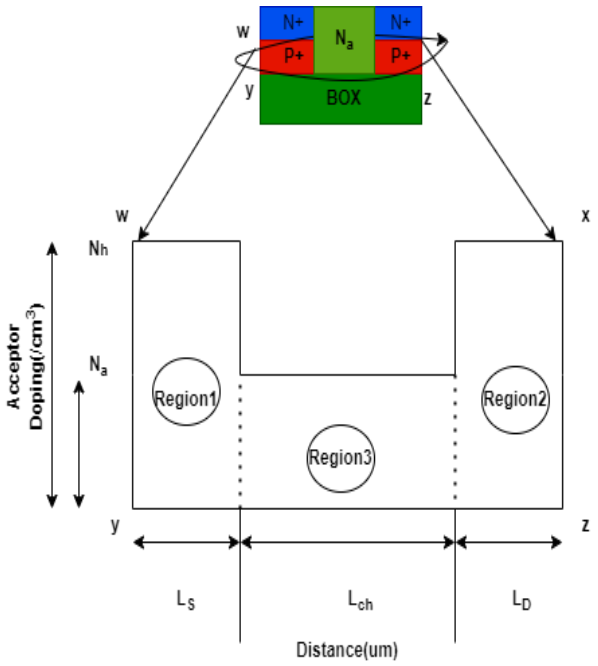

Figure 5. BPA for ZT-TDPDSOI with N+ and P+ below source/drain to estimate the average doping

Table 4. Average doping in bulk region

Doping Type	Doping (cm^{-3})	Factor, F	Average doping (P+) (cm^{-3})	HC (cm^{-3})
P+	2×10^{20}	1333	1.333×10^{20}	5.75×10^{16}
	10^{20}	666	6.66×10^{19}	5.01×10^{16}
	10^{19}	33	3.3×10^{18}	3.89×10^{16}
	10^{18}	6.66	6.6×10^{17}	3.31×10^{16}
	10^{17}	0.6	6×10^{16}	1.81×10^{16}
N+ (Absence of P+)	1×10^{20}	0.3	3×10^{16}	2.39×10^{15}

4.1. Validation of BPA using VBE and FL

The relationship between VBE, FL at drain-channel region and the increased factor is used to validate the estimation of average doping in the bulk region. This is carried out using VBE and FL comparison of PDSOI and ZT-TDPDSOI at drain-channel region in equilibrium given in Figure 2. $E_F - E_V$ is the energy level difference between FL and VBE of PDSOI, given by [3]:

$$(E_F - E_V)_{\text{PDSOI}} = -KT * \ln(\frac{P}{N_v}) \quad (9)$$

where KT is the thermal energy, P is the channel doping concentration, N_v is the valence band density of states. $E_F - E_V$ of PDSOI is −0.335 eV. The average channel doping concentration increases, when P^+ doping is introduced beneath the source/drain regions of PDSOI, leading to a modification of P in Equation (9). The channel concentration increased by a factor f' as shown in Equation (10) as follows:

$$(E_F - E_V)_{\text{ZT-TDPDSOI}} = -KT * \ln(\frac{f' * P}{N_v}) \quad (10)$$

$E_F - E_V$ of ZT-TDPDSOI is −0.134 eV. The distance between VBE and FL of ZT-TDPDSOI is decreased by 0.20 eV.

Subtracting Equation (9) from Equation (10), we get:

$$(E_F - E_V)_{\text{ZT-TDPDSOI}} - (E_F - E_V)_{\text{PDSOI}} = KT * \ln(\frac{1}{f}) \quad (11)$$

The value of f obtained from Section 4 is substituted in Equation (11) and the calculated difference between $E_F - E_V$ of ZT-TDPDSOI and $E_F - E_V$ of PDSOI. This is obtained as 0.187 eV. From the simulator difference between $E_F - E_V$ of ZT-TDPDSOI and $E_F - E_V$ of PDSOI is 0.334−0.134 = 0.2 eV. The details are shown in Table 2. The matching of this result gives the proof that the HC variation is due to the average doping in the bulk region.

Table 5 shows the difference of modelling and simulation for different doping of P^+. ΔE_m is the difference between $E_F - E_V$ of ZT-TDPDSOI and $E_F - E_V$ of PDSOI from Equation (11), and ΔE_s is the difference between $E_F - E_V$ of ZT-TDPDSOI and $E_F - E_V$ of PDSOI for TCAD.

Figure 6 shows the plot of simulation and modelling value of difference between $E_F - E_V$ of ZT-TDPDSOI and $E_F - E_V$ of PDSOI.

Table 5. Modelling and simulation value at drain-channel region for different doping concentrations to validate BPA

Doping (cm^{-3})	ΔE_m (eV)	ΔE_s (eV)	Error (%)
$2*10^{20}$	0.187	0.200	6
10^{20}	0.169	0.180	6
10^{19}	0.109	0.160	6
10^{18}	0.050	0.049	6
10^{17}	-	-	-

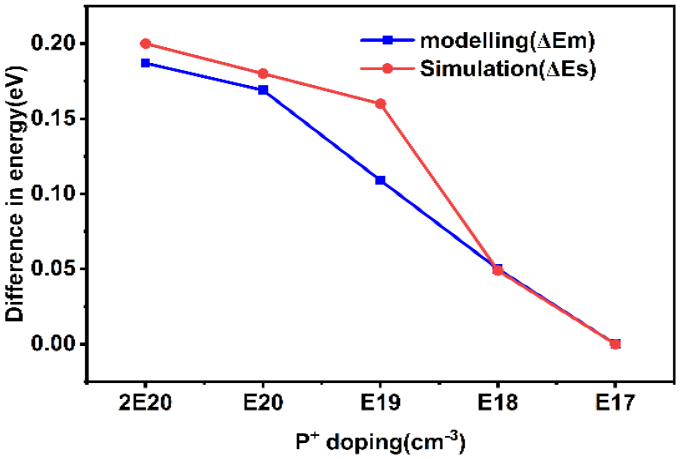

Figure 6. Potential P^+ doping in ZT-TDPDSOI V_{DS} = 1.5 V V_{GS} = 0 V, near the drain-channel region towards N^+P^+ interface to validate BPA

4.2. Ratio of Depletion Capacitance

Depletion capacitance is a crucial parameter which decides SS. The ratio of the SS for PDSOI and ZT-TDPDSOI is calculated from the simulated data. The depletion capacitance analysis is carried out for both PDSOI and ZTTDPDSOI. The SS of PDSOI and ZT-TDPDSOI is given below:

$$\text{SS}_{\text{PDSOI}} = \ln(10) \cdot qkT\left(1 + \frac{C_d}{C_{ox}}\right) \quad (12)$$

$$\text{SS}_{\text{ZT-TDPDSOI}} = \ln(10) \cdot qkT(1 + \frac{C'_d}{C_{ox}}) \quad (13)$$

where C_d is the depletion capacitance of PDSOI and C'_d is the depletion capacitance of ZT-TDPDSOI, C_{ox} is the oxide capacitance. SS_{PDSOI} and $\text{SS}_{\text{ZT-TDPDSOI}}$ obtained from the simulator as 95 mV and 70 mV [15]. This is substituted in Equation (12) and Equation (13). The ratio of Equation (12) to Equation (13) is obtained as 3.5.

$$\frac{C_d}{C'_d} = 3.5 \quad (14)$$

In Figure 7, the potential across channel length is plotted at the middle of the channel for PDSOI and ZT-TDPDSOI. Potential difference at this point is also noted. From the simulator the potential difference at drain-channel at N^+P^+ interface corresponds to PDSOI is 1.2 V and that for ZT-TDPDSOI is 0.381 V. This ratio of this potential difference from Figure 7 is equal to 3.1.

The ratio of AB to CD gives the value 3.1. This is compared to the ratio of C_d/C'_d. The value obtained from the SS equation is 3.5 and the value obtained from simulator is 3.1. The introduction of P+ causes a significant potential variation in ZT-TDPDSOI when compared to PDSOI at the drain-channel region. This is the cause of SS reduction.

$$\frac{AB}{CD} = 3.1 \quad (15)$$

4.3. Relationship of HC with P⁺ Doping

To understand the relationship between HC and P⁺ doping, variation of HC with different doping concentration of P⁺ is carried out as shown in Figure 8. In PDSOI the hole concentration is 2.39 × 10^{13} cm^{-3} at drain-channel junction near the interface of N⁺ and P⁺. Hole concentration is reduced from 10^{17} cm^{-3} to 2.39 × 10^{13} cm^{-3} the reduction factor is 4184. This is due to the movement of holes from channel to N⁺ region. In this case, the average doping in the bulk region is 3 × 10^{16} cm^{-3}. In ZT-TDPDSOI when the P⁺ is 2 × 10^{20} cm^3 the HC increased to 5.75 × 10^{16} cm^{-3} from 2.39 × 10^{13} cm^{-3}, a reduction of factor 1.7 from 10^{17} cm^{-3}. For this case the average doping concentration in the bulk region is 1.333 × 10^{20} cm^{-3}. The average doping is increased from 3 × 10^{16} cm^{-3} to 1.333 × 10^{20} cm^{-3} by a factor 4443. The HC as a function of doping concentration of P⁺ is shown in Figure 8. When the P⁺ doping increases the average doping in the bulk region vary. The HC reaches a maximum value of 5.75 × 10^{16} cm^{-3} near the interface of N⁺ and P⁺ for an average doping of 1.333 × 10^{20} cm^{-3}. It is at this value of average doping; the device attains the minimum SS. Relationship of HC with P⁺ doping from Figure 8 is given by:

$$K' \times P_{p0} = 5 \times 10^{15} \ln(P^+) - 2 \times 10^{17} \quad (16)$$

where P⁺ doping ranges from 2 × 10^{20} cm^{-3} to 10^{17} cm^{-3}. Dependency of HC on doping concentration of P⁺ is logarithmic. *k'* is the scaling factor, P_{P0} equilibrium hole concentration. The doping concentration of P⁺ is varied from 2 × 10^{20} cm^{-3} to 10^{17} cm^{-3} and the hole concentration near the drain region is taken from TCAD and the graph is plotted for this data. The equation is analysed by the curve fitting. The behaviour of HC is shown in Table 4. The equation clearly matches with the data in the 6th column. It is seen that it is varying logarithmically.

5. ELECTRIC FIELD DISTRIBUTION ALONG PP⁺ REGION FOR VARIOUS DOPING OF P⁺

From Poisson's equation, the electric field near drain is [3]:

$$E_{\max PP+} = \frac{qN_A x_p}{\varepsilon_{si}} \quad (17)$$

where q is electron charge, N_A is p-type doping, x_p is depletion width and ϵ_{si} is permittivity of silicon. A horizontal cutline is drawn near N⁺P⁺ interface (0.11 µm), middle of P⁺ region (0.125 µm), at the end of P⁺ and BOX region (0.135 µm) near drain P⁺ junction to get the electric field. Figure 9 shows the electric field distribution at the drain channel junction at different positions 0.11 µm, 0.125 µm, 0.135 µm near drain P⁺ junction for varying doping concentration of P⁺ = 10^{18} cm^{-3}, P⁺ = 10^{19} cm^{-3}, P⁺ = 10^{20} cm^{-3}, and P⁺ = 2 × 10^{20} cm^{-3}. The biasing condition is considered as V_{DS} = 1.5 V and V_{GS} = 0 V. From Figure 9 the electric field is maximum of 255K V/cm for P⁺ = 2 × 10^{20} cm^{-3}, 246K V/cm for P⁺ = 1 × 10^{20} cm^{-3}, 234K V/cm for P⁺ = 1 × 10^{19} cm^{-3}, and 239K V/cm for P⁺ = 1 × 10^{18} cm^{-3}.

Electric field profile at different position N⁺P⁺ interface (0.11 µm), middle of P⁺ region (0.125 µm), at the end of P⁺ and BOX region (0.135 µm) near drain P⁺ of PDSOI is also shown. This confirms the fact that there is negligible electric field variation in conventional PDSOI. Here the maximum electric field is observed at PN⁺ junction which is 196K V/cm. A peak Electric field is observed at N⁺P⁺ interface (0.11 µm), and it decreases toward the edge of the *P*⁺ and BOX region (0.135 µm). It is also observed that electric field increases with increase in doping of P⁺ region. A close association of intense electric field is observed with SS reduction. Maximum local electric field observed near the drain-channel region, is for the doping concentration P⁺ = 2 × 10^{20} cm^{-3}, consequently account for the preferred HC in the bulk region for achieving the capacitance effect thereby reducing the SS in the conventional PDSOI.

5.1. Conduction Band at Drain-Channel Junction at PP⁺ for Varying P⁺ Doping Concentration

Figure 10 shows the conduction band energy at drain-channel junction P⁺P for varying doping concentration of P⁺ at V_{DS} = 0V and V_{GS} = 0 V. A cutline is drawn at PP⁺ junction

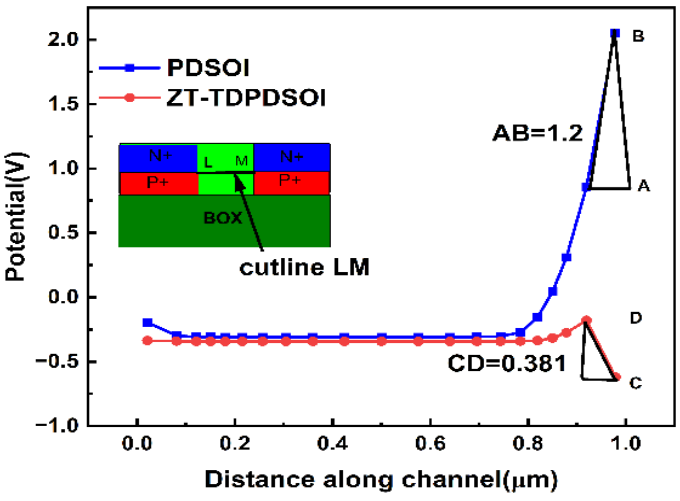

Figure 7. Potential P⁺ doping in ZT-TDPDSOI V_{DS} = 1.5 V V_{GS} = 0 V, near the drain-channel region towards N⁺P⁺ interface, slope at the junction increases from 0.381 to 1.2

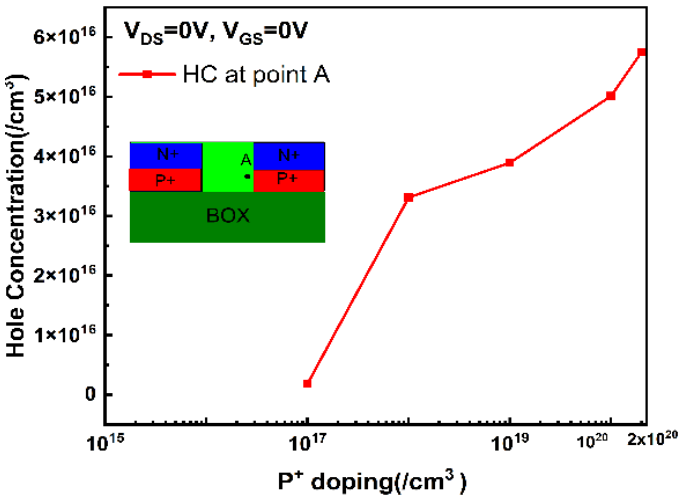

Figure 8. HC as a function of P⁺ doping in ZT-TDPDSOI V_{DS} = 0 V V_{GS} = 0 V, near the drain-channel region towards N⁺P⁺ interface, HC has a logarithmic relationship with P⁺ doping

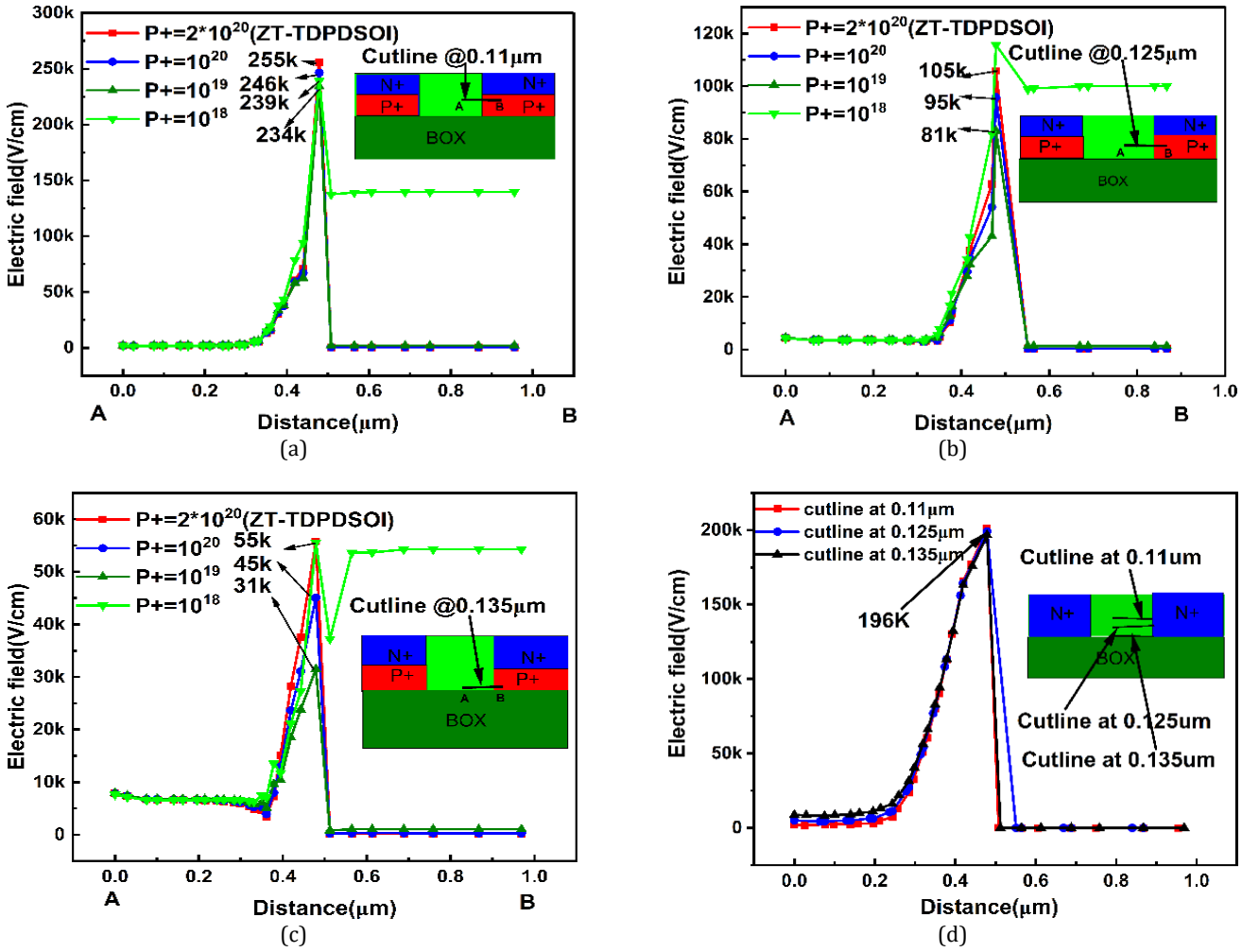

Figure 9. Electric field distribution at different position at PP⁺ junction near drain-channel region for various doping of P⁺. (a) Electric field profile at 0.11 μm near drain-channel region P⁺. (b) Electric field profile at 0.125 μm near drain-channel region PP⁺ varying P⁺ doping for varying P⁺ doping. (c) Electric field profile at 0.135 μm near drain-channel region PP⁺ (d) Electric field profile at different position at N⁺P⁺ for varying P⁺ doping from 10^{18} to 2×10^{20} by drawing a horizontal interface (0.11 μm), middle of P⁺ region (0.125 μm), at the cutline AB end of P⁺ and BOX region (0.135 μm)

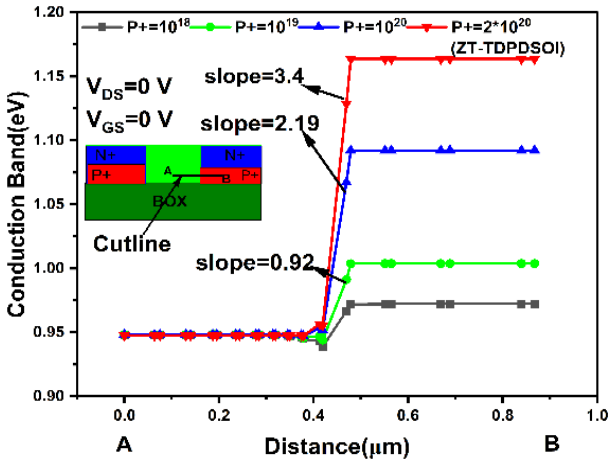

Figure 10. Conduction band at drain-channel junction at PP⁺ for varying P⁺ doping concentration showing the slope at the edge of ZT-TDPDSOI should be higher than 2.19

near drain-channel side to extract the conduction band. The slopes for doping concentration P⁺ = 10^{18} cm^{-3}, P⁺ = 10^{19} cm^{-3}, P⁺ = 10^{20} cm^{-3}, P⁺ = 2×10^{20} cm^{-3} are –0.562, –0.92, 2.2, and 3.4, respectively. The gradient of energy gives the electric field which is represented as slope. The slope corresponding to the doping concentration P⁺ = 2×10^{20} cm^{-3} is seen to be 3.4 V/cm. The slopes of P⁺ = 1×10^{20} cm^{-3} is 2.2 V/cm. There is a 50% increase in the slope with small change in the doping concentration from P⁺ = 1×10^{20} cm^{-3} to P⁺ = 2×10^{20} cm^{-3}. The slope to conduction band energy graph is high at drain-channel junction for doping concentration of P⁺= 2×10^{20} cm^{-3}. This cause guarantees to achieve a capacitance effect in the bulk region, which is the necessary condition for getting the low SS.

5.2. Hole Concentration Near Drain-Channel as a Function of P⁺ Doping

According to Boltzmann approximation, HC is given by [3]:

$$P = n_i * \exp \frac{\phi_b}{V_t} \tag{18}$$

where n_i is the intrinsic concentration, ϕ_b is the bulk potential, V_t is the thermal voltage. Figure 11 shows the HC near drain-channel at PP⁺ for varying doping concentration of P⁺ at biasing condition V_{DS} = 1.5 V and V_{GS} =0 V. Along AB the HC increases as the doping concentration of P⁺ increases. At doping concentration of P⁺ = 10^{18} cm^{-3}, the HC

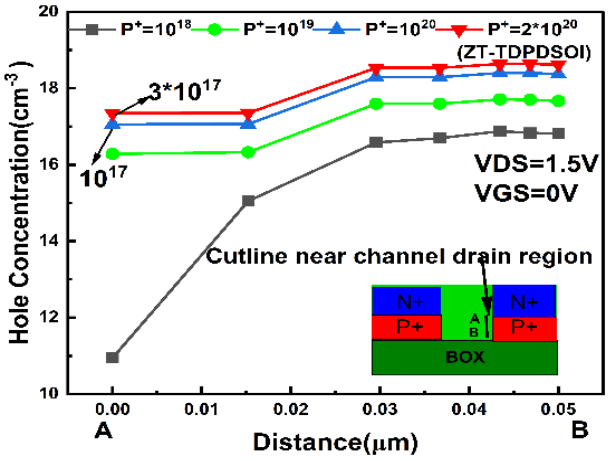

Figure 11. Hole concentration near drain-channel junction at PP⁺ for varying doping concentration at V_{DS} = 1.5 V and V_{GS} =0 V. HC is increasing with doping concentration of P⁺

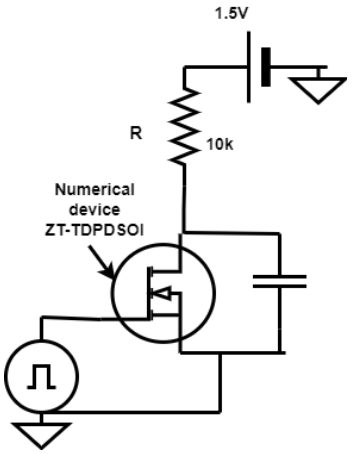

Figure 12. Resistive load inverter using numerically simulated ZT-TDPDSOI, load resistor is 10 KΩ , V_{DS} = 1.5 V

at point A inside the channel becomes more intrinsic since the point is near the interface of N⁺P⁺. As point B is far away from N⁺ and is near to BOX region the HC is increased and reaches a value of 10^{16} cm^{-3}. For P⁺ = 2 × 10^{20} cm^{-3} more HC is induced at point A which is greater than the channel doping (10^{17} cm^{-3}) and at point B HC attains a value equal to 10^{18} cm^{-3} which is a decade greater than the channel doping (10^{17} cm^{-3}). It is implied that an additional variable capacitance effect in the bulk region, which cause the reduction of SS can be achieved if the point A in the channel is seen to be greater than the doping concentration in the channel region. Channel doping is given as 10^{17} cm^{-3}, a concentration higher than this is necessary to achieve the condition for additional capacitance in the bulk region. This condition is attained at a P⁺ doping concentration of 2 × 10^{20} cm^{-3}.

6. IMPLEMENTATION OF INVERTER CIRCUIT USING ZT-TDPDSOI

Figure 12 shows the resistive load inverter using the ZT-TDPDSOI. The validation if ZT-TDPDSOI is done by implementing Resistive load inverter using mixed signal in TCAD. The numerical device ZT-TDPDSOI which was implemented using Altas is used as the pull-down device. Resistor is used as the pull up device. Load resistance R is given as 10 kΩ.

Figure 13 shows the transfer characteristics of inverter circuit. Switching threshold is the point where the transition takes place, from ON to OFF and from OFF to ON. Ideal values of switching threshold should be half of V_{DD}. Switching threshold is increased from 0.4 V to 0 .45 V (12% increase) and the slope increases from 3.91 to 4.08. (4% increase). Details are shown in Table 6. This shows that the inverter using the ZT-TDPDSOI increases the efficiency.

7. CONCLUSION

In conclusion this paper portrays how depletion capacitance variation affects switching threshold and transition slope of an inverter, by demonstrating a prerequisite for modulating the hole concentration (HC) in

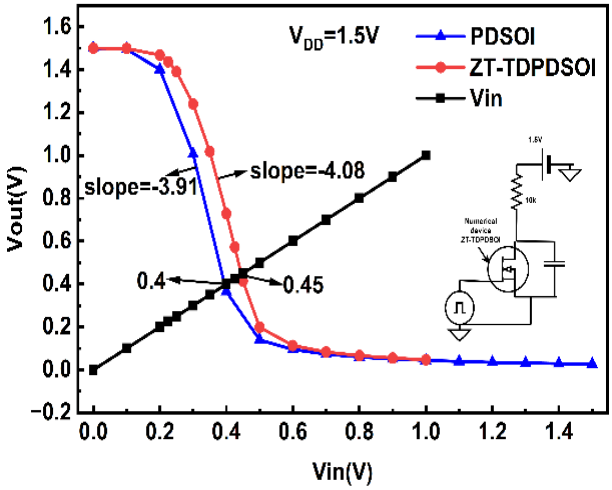

Figure 13. Comparison of Inverter characteristics using ZT-TDPDSOI and PDSOI showing the shift of switching threshold from 0.4 to 0.45

the channel towards the bulk region of ZT-TDPDSOI. The P⁺ below source/drain in Zener Tunnelling Tunnel Diode Partially Depleted Silicon On Insulator Metal Oxide Field Effect transistor (ZT-TDPDSOI MOSFET) modulates the HC in the channel, which helps to achieve a variable capacitance effect that reduces subthreshold swing (SS). The box profile approximation (BPA) validates the average doping in the bulk, modulating the HC. The variations of HC at the drain channel region resulted in the modulation of bulk potential due to P⁺ below source/drain in a ZT-TDPDSOI MOSFET is also revealed here. Thus, assuring the fact that P⁺ region

Table 6. Comparison of rise time, fall time, switching threshold, transition slope of PDSOI and ZT-TDPDSOI inverter

Performance metrics	PDSOI inverter	ZT-TDPDSOI inverter
Rise time (s)	1.88×10^{-10}	1.72×10^{-10}
Fall time (s)	1.89×10^{-11}	1.93×10^{-11}
Switching threshold (V)	0.40	0.45
Transition slope	3.91	4.08

below source/drain changes the average doping concentration inside the channel region which affect the HC at the drain channel region. This results in the SS modulation. The energy band diagram is employed to explain the concentration change inside the channel near drain channel region. The VBE and FL yields HC, which is then used to authenticate with the bulk potential. The BPA is used to assess the effect of P^+ in HC near drain channel region. TCAD simulations are used to validate the model's results. A maximum HC in the bulk region greater than the channel doping, a peak electric field in the middle to the bulk region and also a steep slope of conduction band are the prerequisites for attaining a series variable capacitance effect in the bulk which reduces SS. The present work is primarily based on analytical and simulation studies, in future experimental fabrication and characterization of the proposed structure can be carried out to validate the obtained results under practical operating conditions. Furthermore, detailed RF switch application analysis, including insertion loss, isolation, linearity, power handling capability, and high-frequency reliability assessment, can be explored to evaluate the suitability of the proposed device for modern wireless communication and microwave systems. The proposed structure can be considered for advanced semiconductor and RF integrated circuit technologies where low power and faster switching are desired.

ACKNOWLEDGMENTS

The authors would like to acknowledge the support received from VLSI lab, School of Engineering, Cochin university of Science and Technology for performing the device simulations.

DECLARATIONS

All authors declare that they have no conflicts of interest.

REFERENCES

[1] D. J. Frank, R. H. Dennard, E. Nowak, P. M. Solomon, Y. Taur, and Hon-Sum Philip Wong, "Device scaling limits of Si MOSFETs and their application dependencies," *Proceedings of the IEEE*, vol. 89, no. 3, pp. 259–288, 2001, doi: 10.1109/5.915374.

[2] D. J. Wouters, J.-P. Colinge, and H. E. Maes, "Subthreshold slope in thin-film SOI MOSFETs," *IEEE Transactions on Electron Devices*, vol. 37, no. 9, pp. 2022–2033, 1990, doi: 10.1109/16.57165.

[3] Y. Tsividis, *Operation and Modeling of the MOS Transistor*. in Electrical Engineering Series. McGraw-Hill, 1987.

[4] Y. Taur and T. H. Ning, *Fundamentals of Modern VLSI Devices*, 3rd ed. Cambridge: Cambridge University Press, 2021. doi: DOI: 10.1017/9781108847087

[5] R. S. Muller and T. I. Kamins, *Device Electronics for Integrated Circuits*. Wiley, 2002.

[6] M. Nishida, "Depletion approximation analysis of the differential capacitance—voltage characteristics of an MOS structure with nonuniformly doped semiconductors," *IEEE Transactions on Electron Devices*, vol. 26, no. 7, pp. 1081–1085, 1979, doi: 10.1109/T-ED.1979.19549.

[7] V. K. Aggarwal *et al.*, "Growth of Ge on silicon-on-insulator wafer by plasma enhanced chemical vapor deposition and fabrication of microline photodetector using the Ge layer," *Materials Science and Engineering: B*, vol. 302, p. 117242, 2024, doi: 10.1016/j.mseb.2024.117242.

[8] M. Vardhan and A. J G, "A Comparative analysis of Electrical Characteristics in Bulk, PD, FD and Optimized SOI MOSFETs," in *2024 International Conference on Communication, Computing and Energy Efficient Technologies (I3CEET)*, IEEE, 2024, pp. 566–571. doi: 10.1109/I3CEET61722.2024.10993964.

[9] N. P. Singh *et al.*, "Small signal PD SOI MOSFET model: considering impact ionization and self-heating effects," *Solid-State Electronics*, vol. 229, p. 109200, 2025, doi: 10.1016/j.sse.2025.109200.

[10] P. Harika, Kg. Sravani, G. Shanthi, M. D. B. Jaffery, K. R. Sai, and Sk. S. Vali, "Comprehensive analysis of fully depleted and partially depleted silicon-on-insulator FET device," *Microsystem Technologies*, vol. 31, no. 4, pp. 947–962, 2025, doi: 10.1007/s00542-024-05709-9.

[11] Md. M. Alam, Md. A. Rahman, A. T. Parisa, and T. A. Chowdhury, "Design & Analysis of 5 nm PDSOI and FDSOI n-MOSFETs for Ultra-Low Power Applications with High-k Dielectric Materials," *Materials Sciences and Applications*, vol. 17, no. 02, pp. 35–49, 2026, doi: 10.4236/msa.2026.172003.

[12] M. R. Islam and S. A. Hossain, "Effect of Non-Uniform Doing on Gate C-V Characteristics of MOSFETS," Dhaka, 2010.

[13] J.-P. Colinge, *Silicon-on-Insulator Technology: Materials to VLSI*. Boston, MA: Springer US, 2004. doi: 10.1007/978-1-4419-9106-5.

[14] V. M. Chen and J. C. S. Woo, "Tunneling source-body contact for partially-depleted SOI MOSFET," *IEEE Transactions on Electron Devices*, vol. 44, no. 7, pp. 1143–1147, 1997, doi: 10.1109/16.595943.

[15] J. Chen *et al.*, "A Tunnel Diode Body Contact Structure to Suppress the Floating-Body Effect in Partially Depleted SOI MOSFETs," *IEEE Electron Device Letters*, vol. 32, no. 10, pp. 1346–1348, 2011, doi: 10.1109/LED.2011.2162813.

[16] J. Luo, J. Chen, Q. Wu, Z. Chai, T. Yu, and X. Wang, "TDBC SOI technology to suppress floating body effect in PD SOI p-MOSFETs," *Electronics Letters*, vol. 48, no. 11, pp. 652–653, 2012, doi: 10.1049/el.2012.0980.

[17] M. K. Anvarifard and Z. Ramezani, "A suggested nanoscale partially depleted SOI-MOSFET (PDSOI) by built-in tunneling diodes- improvement on short channel effects and frequency features," *Materials Science and Engineering: B*, vol. 296, p. 116612, 2023, doi: 10.1016/j.mseb.2023.116612.

[18] S. Dutta, T. Chavan, N. R. Mohapatra, and U. Ganguly, "Electrical Tunability of Partially Depleted Silicon on Insulator (PD-SOI) Neuron," *Solid-State Electronics*, vol. 160, p. 107623, 2019, doi: 10.1016/j.sse.2019.107623.

[19] S. Baby, G. B. Vincent, and A. Pradeep, "OFF Current Reduction using Zener Tunneling in Tunnel Diode Body Contact Silicon On Insulator," in *2022 IEEE International Conference on Nanoelectronics, Nanophotonics, Nanomaterials, Nanobioscience & Nanotechnology (5NANO)*, IEEE, 2022, pp. 1–6. doi: 10.1109/5NANO53044.2022.9828929.

[20] S. Baby and A. Pradeep, "Reduction of Subthreshold Swing in Zener Tunnelling-Tunnel Diode Partially Depleted Silicon On Insulator," in *2022 International Conference on Futuristic Technologies (INCOFT)*, IEEE, 2022, pp. 1–5. doi: 10.1109/INCOFT55651.2022.10094540.

[21] S. Baby, A. Pradeep, and U. S. Shikha, "Investigation of junction capacitance in Zener tunnelling tunnel diode partially depleted silicon on insulator," *Micro and Nanostructures*, vol. 186, p. 207729, 2024, doi: 10.1016/j.micrna.2023.207729.

[22] D. Nandi *et al.*, "Utilizing Symmetric BSIM-SOI SPICE Model for Dynamically Depleted RF SOI T/R Switches and Logic Circuits," *IEEE Journal of the Electron Devices Society*, vol. 13, pp. 800–807, 2025, doi: 10.1109/JEDS.2024.3484295.

[23] D. Nandi *et al.*, "Validation of Dynamically Depleted Symmetric BSIM-SOI Compact model for RF SOI T/R Switch Applications," in *2024 8th IEEE Electron Devices Technology & Manufacturing Conference (EDTM)*, IEEE, 2024, pp. 1–3. doi: 10.1109/EDTM58488.2024.10512295.

[24] D. Germano Alves Neto *et al.*, "Design-Oriented Single-Piece 5-DC-Parameter MOSFET Model," *IEEE Access*, vol. 12, pp. 87420–87437, 2024, doi: 10.1109/ACCESS.2024.3417316.

[25] B. D. R. Bonkoungou, R. Gwoziecki, G. Perez, L. Sterna, and Z. Khatir, "Optimized semi-physical EKV model for simulation of SiC MOSFETs," *Microelectronics Reliability*, vol. 171, p. 115780, 2025, doi: 10.1016/j.microrel.2025.115780.

[26] H.-C. Cheng, W.-Y. Jhu, Y.-C. Liu, C.-F. Yu, P.-K. Chiu, and T.-C. Chang, "Effects of parasitic capacitance on switching transients and thermal performance in a single-phase SiC power MOSFET inverter," *Scientific Reports*, vol. 16, no. 1, p. 13537, 2026, doi: 10.1038/s41598-026-44458-9.

[27] SILVACO, Inc., *ATLAS User's Manual: Device Simulation Software*. Santa Clara, CA, USA: SILVACO, Inc., 2010.